1999202624 420195 A 12P

Soot Aerosol Properties in Laminar Soot-Emitting Microgravity Nonpremixed Flames

BOGDAN KONSUR, CONSTANTINE M. MEGARIDIS

Department of Mechanical Engineering (M/C 251), University of Illinois at Chicago, 842 W. Taylor Street, Chicago, IL 60607-7022, USA

PREPRINT IN-25 (Unwaived/CASI)

and

DEVON W. GRIFFIN

Microgravity Fluid Physics Branch, MS 110-3, NASA Lewis Research Center, 21000 Brookpark Rd., Cleveland, OH 44135, USA

The spatial distributions and morphological properties of the soot aerosol are examined experimentally in a series of 0-g laminar gas-jet nonpremixed flames. The methodology deploys round jet diffusion flames of nitrogen-diluted acetylene fuel burning in quiescent air at atmospheric pressure. Full-field laser-light extinction is utilized to determine transient soot spatial distributions within the flames. Thermophoretic sampling is employed in conjunction with transmission electron microscopy to define soot microstructure within the soot-emitting 0-g flames. The microgravity tests indicate that the 0-g flames attain a quasi-steady state roughly 0.7 s after ignition, and sustain their annular structure even beyond their luminous flame tip. The measured peak soot volume fractions show a complex dependence on burner exit conditions, and decrease in a nonlinear fashion with decreasing characteristic flow residence times. Fuel preheat by ~140 K appears to accelerate the formation of soot near the flame axis via enhanced fuel pyrolysis rates. The increased soot presence caused by the elevated fuel injection temperatures triggers higher flame radiative losses, which may account for the premature suppression of soot growth observed along the annular region of preheated-fuel flames. Electron micrographs of soot aggregates collected in 0-g reveal the presence of soot precursor particles near the symmetry axis at midflame height. The observations also verify that soot primary particle sizes are nearly uniform among aggregates present at the same flame location, but vary considerably with radius at a fixed distance from the burner. The maximum primary size in 0-g is found to be by 40% larger than in 1-g, under the same burner exit conditions. Estimates of the number concentration of primary particles and surface area of soot particulate phase per unit volume of the combustion gases are also made for selected in-flame locations.

INTRODUCTION

Nonbuoyant flames offer a relatively unexplored platform to improve understanding of soot mechanisms [1]. The effects of buoyancy are eliminated temporarily in drop towers, which sustain brief intervals of reduced gravity—typically lower than 10^{-3} g—extending up to several seconds at a time. Such an environment is referred to as microgravity or 0-g. Microgravity facilities have been employed [2] to show that nonbuoyant hydrocarbon flames are longer, wider, and sootier than their normal-gravity counterparts.

Mortazavi et al. [3] established that residence times in microgravity laminar jet nonpremixed flames with $Re = O(100)$ tend to be proportional to burner diameter and inversely proportional to burner exit velocity. This offers great flexibility in altering residence times in these flames by manipulating the burner exit diameters and velocities. Conversely, flame residence times in the corresponding normal-gravity flames are rather limited, since they are controlled largely by buoyancy.

The soot-field structure within laminar microgravity gas-jet nonpremixed flames has been examined by Megaridis et al. [4] for flames operated well above their smoke point. The fuel was nitrogen-diluted (50% vol.) acetylene burning in quiescent air at atmospheric pressure. The work was conducted at the 2.2-second drop tower of the NASA Lewis Research Center (NASA-LeRC). As reported in [4], the soot fields in 0-g sustained a

Corresponding author. E-mail: cmm@uic.edu

COMBUSTION AND FLAME 118:509–520 (1999)

Published by Elsevier Science Inc.

0010-2180/99/$–see front matter
PII S0010-2180(99)00021-8

pronounced annular structure throughout the luminous nonbuoyant-flame zone. This finding establishes that the annular structure of the soot field in laminar coflow nonpremixed flames is not caused by buoyancy. In [4], the maximum soot volume fraction measured at 0-g was nearly a factor of 2 higher than that at 1-g. A follow-up study by the same investigators [5] examined the effect of moderate fuel preheat on the structure of the soot fields. Greenberg and Ku [6] presented identical trends for flame conditions similar to those considered in [4]. The above studies [4–6] clearly demonstrated the improved spatial resolution afforded in microgravity flames compared to their normal-gravity counterparts. Just recently, the first long-duration 0-g experimental study of soot processes was performed in space [7]. The work produced a wealth of experimental data, which included luminous flame shapes, soot concentration distributions, soot and gas temperature distributions, soot structure, and flame radiation. The above set of measurements was performed at atmospheric and half-atmospheric pressure.

The present work extends the 0-g flame soot mea- surements reported in [4] and [5], by adding new 0-g data for different fuel flow rates and burner diameters. Some measurements, which ap- peared in [5], are also repeated herein for clarity and in order to facilitate comparisons with the data obtained for the added experimental conditions. These new flame conditions allow more conclusive comparisons regarding the effect of characteristic flow residence times on soot-field structure, the influence of fuel preheat on fuel pyrolysis rates near the flame centerline, and the premature cessation of soot growth along the soot annulus in 0-g when the fuel is preheated. Furthermore, this paper reports on the implementation of thermophoretic soot sampling in a specific 0-g flame featuring burner exit velocities typical of buoyant flames, and presents quantitative data on the radial variation of soot microstructure at a fixed height above the burner mouth. Soot primary particle sizes in 1-g and 0-g are also presented and compared to previously published values.

EXPERIMENTAL CONDITIONS AND METHODS

Flame Conditions

The laminar gas jet nonpremixed flames investigated in this study were operated at atmospheric pressure in a rectangular enclosure with dimensions 30 cm × 21 cm × 43 cm. The flames were anchored either on a 1.6 mm or 1.2 mm inner-diameter stainless-steel burner, which was positioned vertically in the chamber. The round burner tip was positioned approximately 50 mm above a flat base plate which held the nozzle and the spark ignitor assembly. The nozzle length-to-diameter ratio was around 55 to ensure that fully developed flow emerged from the burner tip. The fuel mixture consisted of 50% (volume) C_2H_2–50% N_2 and was issued into quiescent air at room temperature. The base fuel flow rate of 2.2 mg/s (corresponding to a volume flow rate of 2 cm^3/s at room temperature and atmospheric pressure) was selected as defining flame sizes that provided adequate resolution of the soot fields both in 1-g and 0-g, as well as short transients after ignition in microgravity [4]. Experiments were also conducted at two lower fuel flow rates, namely 1.2 mg/s and 1.6 mg/s. In addition to the unpreheated-fuel conditions, one preheated-fuel configuration (fuel exit temperature of 160°C) was examined for the base mass flow rate of 2.2 mg/s. Fuel preheat was utilized as a means to vary the flame residence time in 0-g under a fixed mass flow rate. Table 1 lists five burner exit conditions for the flames studied in this work. All burner exit conditions listed in this table produced nonflickering flames in normal gravity as well as within the 2.2-s period available for measurements in microgravity. All 1-g flames emitted no soot from their closed conical tip, whereas their nonbuoyant counterparts released soot from their open tip. The smoke point of the diluted unpreheated acetylene fuel at 0-g was determined to be in the range from 0.77 to 1.1 mg/s (0.7 to 1 cm^3/s at room temperature and atmospheric pressure). The above confirms the findings of Urban et al. [7] who reported that the laminar smoke point flow rates in 0-g are significantly

TABLE 1

Flame Operating Conditions

Case	Burner Diam. (mm)	Fuel Exit Temp. (deg. C)	Fuel Flow rate (mg/s)	Fuel Flow rate [cm^3/s]	Mean Exit Velocity (cm/s)	Exit Re	0-g Luminous Height (mm)	1-g Luminous Height (mm)
I	1.6	23	1.6	[1.5]	74.6	96	19.0	16.9
II[a]	1.6	23	2.2	[2.0]	99.5	128	28.3	26.4
IV	1.6	160	2.2	[2.9]	145.5	98	26.5	26.0
V	1.2	23	2.2	[2.0]	186.2	174	26.6	24.0
VI	1.6	23	1.2	[1.1]	54.6	70	14.6	9.0

[a] Base case.

lower than those of the buoyant flames burning the same fuel. As suggested in [4] and verified in [7], this is a result of the extended residence times in 0-g which cause prolonged growth without compensating increases in soot oxidation. The cessation of the soot oxidation processes in 0-g occurs by quenching near the flame tip, as shown by the temperature measurements reported in [7].

Apparatus

The experimental rig is the same one used in our previous studies [4, 5] which were conducted in the 2.2-s drop tower of the NASA-LeRC. Detailed information on the drop tower facility can be found in [8]. Each microgravity experiment lasts for 2.2 s, during which data are collected continuously. A typical drop sequence starts with the rig release from the top of the tower (onset of microgravity), and proceeds with fuel flow initiation, ignition (via spark), flame development, and finally, impact on an airbag at the bottom of the tower (end of 2.2-s-long microgravity period). Diagnostic instrumentation includes direct video imaging of the flame and laser-light extinction for determination of soot volume fraction distributions (see below). The luminous flame emission is recorded throughout each drop. Experiments are fully automated, powered by DC current and are controlled via an onboard computer. Further details on the experimental apparatus are given in [4, 5] and are not repeated herein for brevity.

Measurement of Soot Distributions via Full-Field Laser-Light Extinction

Soot volume fraction distributions within the flames were determined via a full-field laser-light extinction technique [9] which is based on principles of optical tomographic reconstruction and is capable of determining transient soot spatial distributions in laminar axisymmetric flames. The capability of this technique to follow time-dependent fields is essential in microgravity flames because of their transient character after ignition in 0-g. The instrumentation for these measurements has been described in detail in [4]. In this technique, a laser light beam (λ = 674.9 nm) is spatially filtered, expanded and collimated to a cylinder approximately 50 mm in diameter before passing through the soot-laden flame. Soot scatters and absorbs light depending on the particle size, producing a shadow-like image at the back of the flame [5]. Such images viewed by a CCD camera through a laser-line filter are recorded at a rate of 30 frames per second and are used for data reduction after the completion of each 0-g experiment. Raw soot-field images are postprocessed according to the techniques described in [4]. When the image frame of the soot field at a specific instant is compared to a reference frame taken before the flame was ignited, the instantaneous line-of-sight fractional absorption can be calculated after an appropriate correction for flame luminosity [4]. Typical absorption levels in the flames investigated are of the order of 25%, being occasionally as high as 35%, thus satisfying the optically thin medium assumption. From each horizontal intensity profile (Z =

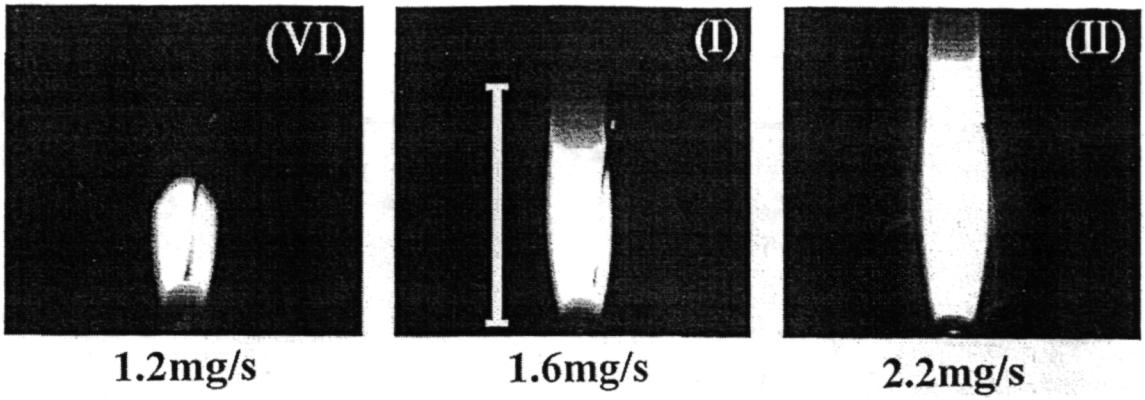

Fig. 1. Luminous flame images in 0-g: VI) lowest flow rate, I) intermediate flow rate, and II) highest (base) flow rate. These images were captured after the brief initial transients in 0-g and correspond to a quasi-steady state. The illuminated burner tip can be seen at the base of each flame image. The spark ignition wires are also visible in Flames VI and I. These wires were in the field of view, but were positioned far enough from the flame to minimize interference with the combustion process. The vertical scale drawn in (I) corresponds to a length of 25 mm. Photographs I and II have been reproduced from [5].

constant), the radial distribution of soot volume fraction is determined using a three-point Abel deconvolution algorithm [10], and Rayleigh scattering theory with a specific value of the refractive index of soot (1.57–0.56 i) [11]. As discussed in [5], discrepancies between the Rayleigh approximation and the more detailed Rayleigh-Debye-Gans (RDG) scattering theory are largest at short wavelengths (~500 nm) for heavily sooting fuels. The moderate laser wavelength of the current work (674.9 nm) suggests that these discrepancies are not significant, especially when compared to uncertainties in soot refractive index [12]. The soot volume fraction distributions reported in the following have been symmetrized with respect to the flame axis.

Measurement of Soot Morphology via Thermophoretic Soot Sampling and Transmission Electron Microscopy

Soot microstructure was examined using thermophoretic sampling, a technique that has been shown [13, 14] to provide an accurate representation of the morphological character of flame-born aerosols. This method is based on the phenomenon of thermophoresis, which drives the flame-born soot to the cold surface of a precisely positioned probe, where it is ultimately captured. The thermophoretic probe supports a 200-Å-thick elemental carbon substrate that provides a fine background for high-resolution observations using transmission electron microscopy (TEM). In summary, thermophoretic sampling collects soot microsamples from well-defined flame coordinates, and allows subsequent morphological characterization using TEM and image analysis techniques.

RESULTS AND DISCUSSION

Luminous Flame Appearance

Although visible flame appearance does not define the reaction zone in a spatial sense, it provides a reliable means of evaluating the transient character of flames after ignition. Throughout this study, ignition in 0-g occurred consistently at 0.3 s into the 2.2-s-drop sequence. As also reported in [4, 5], video observations of luminous flame zone development showed the initial transients to be complete about 1 s after the onset of microgravity (i.e., 0.7 s after ignition). All flames appeared to remain unchanged thereafter and until 1.7 s–1.8 s into a 0-g experiment, when some pulsing was caused by the established contact between the experiment rig and the drag shield encasing the rig.

Figure 1 displays the luminous images for Flames VI, I, and II (see Table 1), as captured in 0-g after the brief initial transients. The images of I and II are reproduced from [5], and

are repeated here to display the effect of fuel flow rate in 0-g. As seen in this figure, the flame streamwise dimensions appear to increase with flow rate (left to right). It is interesting to note that the maximum diameter of all three flames displayed in Fig. 1 is nearly the same (6–7 mm). This diameter was characteristic of all 0-g flames examined in this work. As argued in [7], the characteristic transient postignition period of a 0-g flame can be estimated by the ratio R^2/D, where R is the maximum luminous flame radius and D is the characteristic mass diffusion coefficient. Considering a value of $D = 40$ mm^2/s (characteristic of a temperature ~1050 K), we calculate a transient period of the order of 1 s, which is consistent with our experimental observations. The relatively short transient development times in the 0-g flames studied herein offer these flames as suitable platforms for soot measurements at the 2.2-s drop tower of the LeRC. The 0-g ethylene flames studied by Urban et al. [7], which were also based on a 1.6-mm-diameter tube burner, had a maximum luminous diameter around 14 mm. The larger sizes of those flames resulted in the passing of several seconds before a quasi-steady state was reached [7], thus requiring a space-based platform where extended periods of 0-g are available.

The luminous flame zones shown in Fig.1 display a fundamental difference between Flame VI (flow rate 1.2 mg/s) and Flames I and II (1.6 and 2.2 mg/s, respectively). Both Flames I and II have an open tip with little or no soot emitted from the centerline, whereas Flame VI appears to contain at its tip substantial amounts of soot near the axis. This behavior is characteristic of flames operating slightly above the smoke point, as also discussed by Urban et al. [7]. Although the soot-emitting character of all 0-g flames examined in this work made the determination of a visible height a dubious task (notice the gradual darkening of flame tip with height in Fig. 1), a flame height was determined as the distance between the burner tip and the axial location where darkening of the luminous zone started to occur. On the other hand, the corresponding flame heights in 1-g were easier to measure because of the closed tip of the 1-g flames [5]. Table 1 lists the luminous flame heights determined in this manner. Naturally, luminous flame height increases with fuel flow rate both in 0-g and 1-g. Also, for a fixed mass fuel flow rate of 2.2 mg/s (Flames II, IV, and V), the flame height remains insensitive to the fuel exit conditions both in 0-g and 1-g. Furthermore, for the fuel rate of 2.2 mg/s, gravity appears to play only a minor role in flame height, as demonstrated by the similar values of this quantity for Flames II, IV, and V in 0-g and 1-g. For the intermediate flow rate of 1.6 mg/s (Case I), some difference is seen in the flame height between 0-g and 1-g. Finally, this difference becomes even more pronounced at the lowest flow rate 1.2 mg/s (Case VI).

0-g Soot Fields

The radial distributions of soot volume fraction (f_v) were determined at distinct axial stations above the burner tip for the first four flames listed in Table 1. The specific heights where distributions were produced ranged from Z = 10 mm to 30 mm, in 5-mm increments. Comparisons of the soot fields in Flames I, II, and IV have been reported in [5] and will not be repeated here. In the following, soot distribution comparisons are made for Flames II, IV, and V, in order to provide insight on the influence of two factors, namely, fuel preheat and characteristic flow residence times. As discussed in [5], fuel preheat by ~100 K may cause significant changes in fuel pyrolysis rates, thus affecting soot formation rates. Furthermore, in jet diffusion flames burning in 0-g with Re = O(100), residence times scale proportionally to burner diameter and inversely proportional to fuel exit velocity [3]. Consequently, flow residence times in Flames IV and V should be by 32% and 60% (respectively) lower than those in the base flame (II).

Figure 2 displays the radial variations of f_v at two selected axial heights (Z = 20 mm, 30 mm) in Flames II, IV, and V. The distributions for Flames II and IV are reproduced from [5] to facilitate comparison. The location Z = 30 mm lies slightly beyond the point defining the flame luminous height for each flame (see Table 1). At both heights, the soot distributions display a well-defined annular structure, which is maintained even past the flame tip (see Fig. 2B). It is seen, though, that the annular character of the

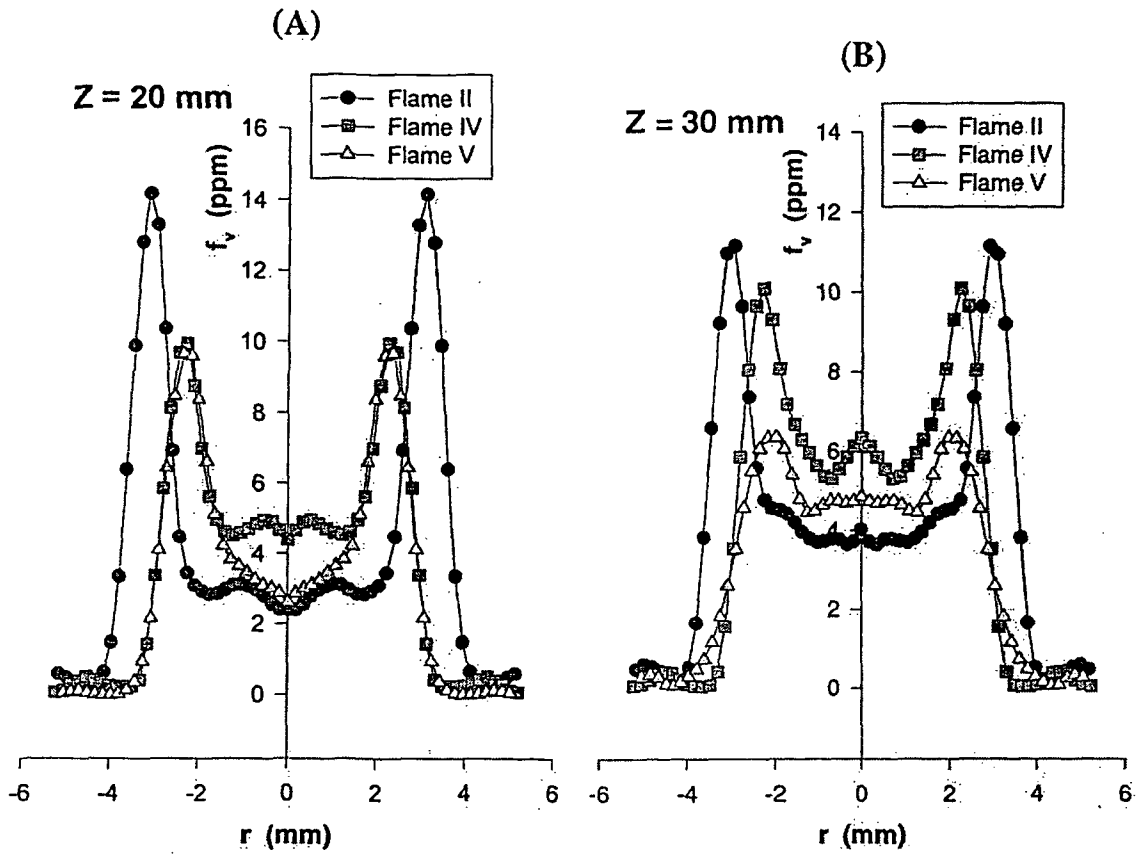

Fig. 2. Radial distributions of soot volume fraction f_v at two distinct axial stations (A at Z=20 mm; B at 30 mm) above the burner mouth of three microgravity flames (II, IV, and V; see Table 1). These radial distributions represent the apparent steady state of the flames following the initial soot-field transients after ignition. The distributions for II and IV have been reproduced from [5].

soot field near the flame tip is weaker in the smaller-burner-diameter flame (V). Similar confinement of the soot aerosol in an annulus near the flame tip was also reported by Honnery and Kent [15] for their long ethylene/air buoyant jet diffusion flames. Therefore, the persistence of the soot annular structure beyond the luminous flame tip cannot be attributed to the nonbuoyant character of the flames investigated herein, but appears to be characteristic of fuel flow rates that are sufficiently higher than the smoke point, irrespectively of the presence of gravity [5]. Figure 2 clearly shows that soot formation occurs along the axis of the three flames. On the other hand, the nonbuoyant ethylene flame investigated by Urban et al. [7] at atmospheric pressure showed no signs of soot formation in the vicinity of the flame axis. This difference may be caused by the larger radial extent of the ethylene flame studied in [7], as well as the different sooting propensity of ethylene compared to the C_2H_2/N_2 mixture used in the current work. Figure 2 also shows that as fuel exit velocities increase from Flame II to IV (see Table 1), the soot annulus moves closer to the symmetry axis. This observation emphasizes the importance of jet momentum in flame structure in 0-g. Finally, the soot-releasing character of the three flames is confirmed by the nonzero value of f_v above the flame tip (Z = 30 mm).

The gradual evolution of the soot aerosol along two characteristic particle paths in Flames II, IV, and V was followed by plotting f_v vs. Z along these paths. Unfortunately, due to the unavailability of velocity fields in these 0-g flames, a f_v vs. t relationship could not be deduced. Figure 3A displays the f_v vs. Z variation along the soot annulus; Fig. 3B follows soot

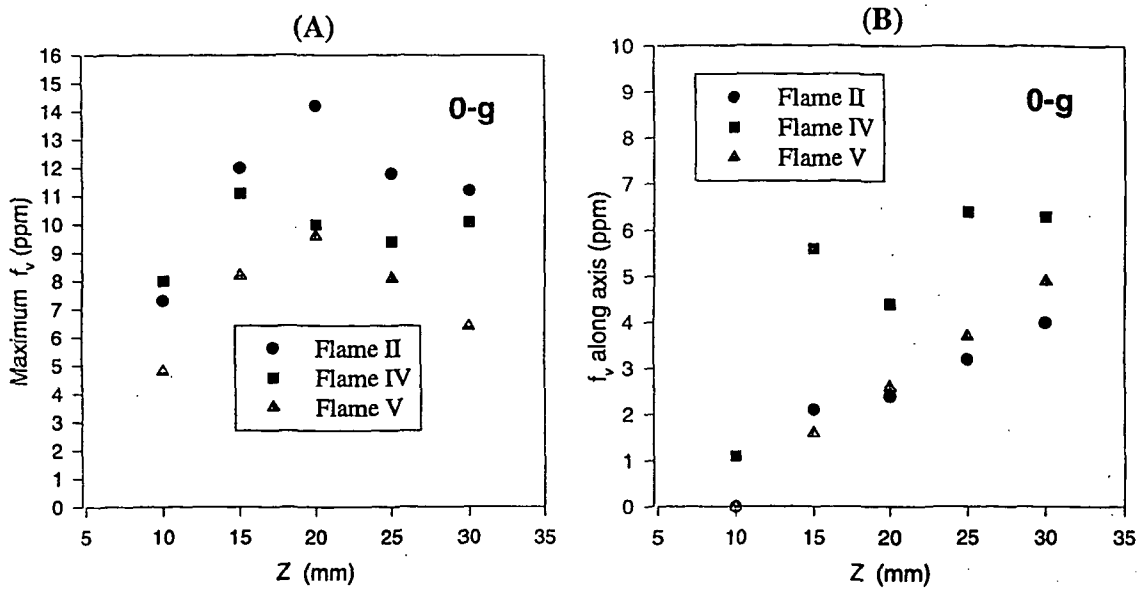

Fig. 3. Comparison of the variation of soot volume fraction along: (A) the soot annulus, and (B) the flame centerline of three 0-g flames. The data points for Flames II and IV have been reproduced from [5].

transport along the symmetry axis. The data points for Flames II and IV are reproduced from [5] and are repeated here to facilitate comparisons.

Figure 3A shows that the soot concentrations in the annuli of Flames II and IV are similar early on (Z <15 mm), suggesting a relatively small influence of the utilized fuel preheat on soot inception rates along the annular region. However, the soot growth rates appear to be slower for Flame IV. This is probably due to the reduced residence times available for growth in this preheated-fuel flame. The corresponding data points for the unpreheated-fuel flames (II and V) follow a parallel ascending/descending trend, but the values of f_v in the base flame (II) remain consistently higher. This disparity in soot volume fractions—despite the same fuel flow rate—may be due to the significantly lower residence times of Flame V compared to the base flame (as stated earlier, flow residence times in Flame V are estimated to be by 60% lower than those in Flame II). Figure 3A also shows that the overall maximum value of f_v declines as residence times decrease from Flame II to V. It is worth noting, however, that the reductions in f_v do not scale with the corresponding residence time reductions, thus attesting to the complexity of the processes involved.

It is also important to note that the peak soot volume fraction in the preheated-fuel flame (IV) occurs at Z = 15 mm, compared to 20 mm in the two unpreheated-fuel flames (II and V). The shift of $(f_v)_{max}$ to lower heights (or likewise, earlier residence times) has been observed in [5] and cannot be attributed to a residence time effect; compared to Flame II, Flame V has an even lower residence time than Flame IV. This shift marks an important difference between unpreheated and preheated-fuel flames in 0-g. A possible explanation for this shift is given in the following paragraph.

Figure 3B reveals interestingly that soot concentrations in the flame core are very similar for both unpreheated-fuel flames (II and V), despite the substantially differing (by ~60%) residence times in these two flames. Because of the relatively higher soot volume fractions in the soot annulus of Flame II (see Fig. 3A), the temperatures in that flame are expected to be lower than those in Flame V. Thus, the soot-suppressing effect of lower temperatures in Flame II could potentially neutralize the soot-promoting influence of longer residence times along the axis of that flame, as compared to Flame V. Figure 3B also shows that the soot volume fractions along the axis of Flame IV (preheated) are considerably higher than those

of the unpreheated-fuel flames. This strong soot-enhancing influence of fuel preheat along the flame centerline cannot be attributed to a residence time effect, because Flame IV features shorter residence times compared to Flame II. As suggested in [5], fuel preheat by O(100 K) appears to enhance fuel pyrolysis rates in the cool flame regions, although such preheat levels correspond to an increase in adiabatic flame temperature of less than 10 K (estimated by taking molecular dissociation into consideration). In turn, enhanced fuel pyrolysis rates accelerate the formation of soot, and may explain the trends seen in Fig. 3B. Nevertheless, the increased soot presence near the axis of the preheated-fuel flame (IV) would cause higher radiative losses, thus reducing flame temperatures and eventually suppressing soot growth [16]. This mechanism may be responsible for the premature (15 mm vs. 20 mm in Fig. 3A) cessation of soot growth seen for the particles transported along the soot annulus of the preheated fuel flame.

Soot Morphology

It has been established that soot aggregates transported in steady buoyant laminar hydrocarbon/air nonpremixed flames consist of primary particles of approximately spherical shape and which, for a specific location within the flame, are of nearly uniform diameter d_p [17]. However, the size of the primary particles as well as the degree of agglomeration (quantified by the number of primary particles per aggregate) are strongly influenced by the position within the flame. It is noted that none of the above findings have been verified for soot aggregates formed and transported in 0-g flames.

The relatively low gas-flow velocities in 0-g flames, as compared to their 1-g counterparts, pose a formidable challenge for the implementation of *ex situ* techniques, such as thermophoretic sampling. These low velocities extend the dissipation period of flame disturbances induced by the probe motion during insertion, thus degrading position correspondence between probe and flame coordinates. Experience from extensive sampling tests in buoyant flames (see [13] and [17]) has established that when thermophoretic sampling is employed unsuccessfully: (a) the collected soot aggregates may contain widely disparate primary sizes d_p, and (b) the radial variation of d_p at a fixed height may be inconsistent and nonreproducible. Ku et al. [18], who first examined the morphology of soot collected thermophoretically in 0-g from propane and ethylene flames, reported large variations of d_p even within individual aggregates. On the other hand, Urban et al. [7] sampled a nonbuoyant ethylene flame and reported that insertion of the thermophoretic sampler caused a significant cross-stream disturbance to the flame, thus rendering the radial variations of soot morphology unreliable. Nonetheless, the latter investigators demonstrated uniformity of soot primary sizes per aggregate for soot collected *beyond* the flame tip [7]. The above implications reaffirm the need for *in situ* optical measurement methods that are capable of providing soot morphological data in flames; see [19] and references cited therein.

In the current study, the elevated fuel exit velocities of Flame IV facilitated the reliable deployment of thermophoretic sampling in 0-g. In principle, high gas-flow velocities result in rapid recovery of the disturbed flame after probe insertion, thus improving spatial position correspondence between probe and flame coordinates, a critical requirement in thermophoretic soot sampling. The burner exit velocity in Flame IV of the current study is 145.5 cm/s (mean value), which is nearly by a factor of 2 higher than the velocities employed in [7] as well as in [18]. It is also noted that this exit velocity is in the range encountered in buoyant flames [20].

Figure 4 displays transmission electron photomicrographs of soot aggregates collected from a height Z = 15 mm of Flame IV in 0-g. This axial height corresponds to the overall peak value of f_v measured in this flame (see Fig. 3A). The micrographs of Fig. 4 depict soot morphology at three radial locations, namely, (A) $r \approx 0.8$ mm; (B) $r \approx 2.3$ mm; and (C) $r \approx 2.8$ mm. In effect, these micrographs represent soot microstructure near the flame axis (A), on the soot annulus (B), and outside the soot annulus (C). Figure 4A (flame axis) reveals the presence of small diffuse background particles, identified as soot precursor particles in [21, 22]. These particles appear to coexist with larger aggregates

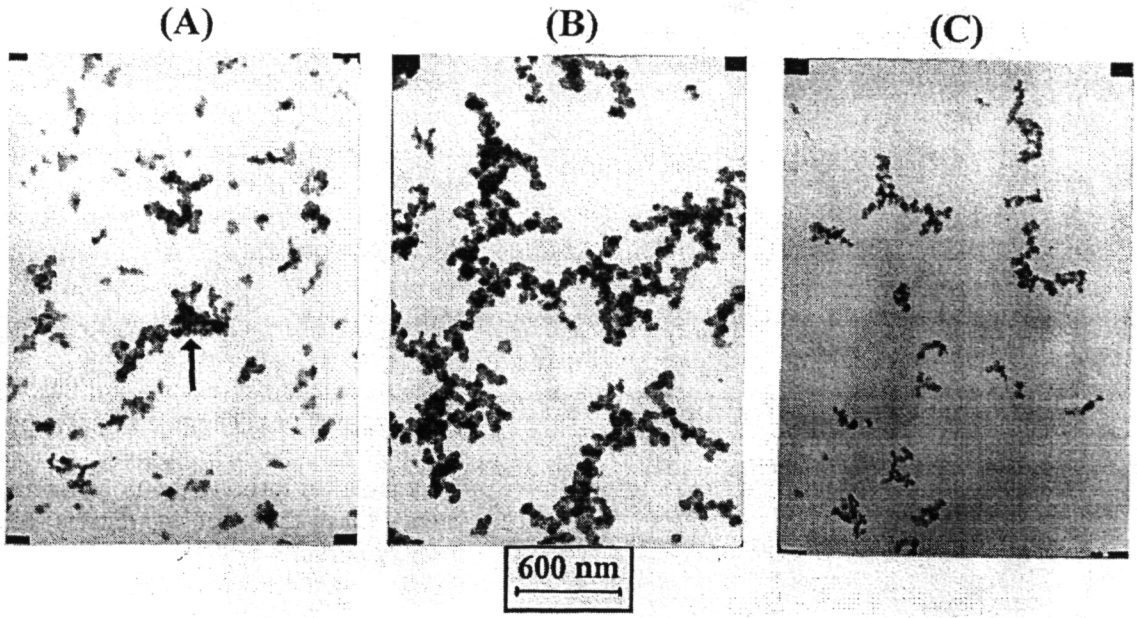

Fig. 4. Transmission electron micrographs of soot aggregates collected from the axial height Z=15 mm of Flame IV in 0-g. This height corresponds to the overall peak value of f_v measured in this flame. The three micrographs depict soot morphology at radial locations (A) near the flame axis, (B) on the soot annulus, and (C) outside the soot annulus. The aggregate identified by the arrow in (A) was probably collected when the thermophoretic probe pierced through the high-density soot annulus.

(see arrow) which were presumably collected when the thermophoretic probe pierced through the high-density soot annulus. The aggregates extracted from the annular region (Fig. 4B) display a rather uniform primary size, as do the aggregates collected further away from the soot annulus (Fig. 4C). While soot primary particle size is uniform for each radial location at this height, it varies noticeably with radius. It is also noted that the observed uniformity of d_p at a fixed location within a 0-g flame, although not surprising in view of our knowledge of 1-g flames, is important because it simplifies the data reduction procedures when optical measurements utilizing the fractal aggregate concept are employed [23–25]. The primary sizes for the soot aggregates of Figs. 4B and 4C were quantified via image analysis. A population of ~150 primary particles was examined at each location using a Micro-Comp high-resolution interactive morphometry station. The values d_p = 40.6 nm (standard deviation σ_g = 5.4 nm) and 29.9 nm (σ_g = 4.8 nm) were determined for the flame locations corresponding to Figs. 4B and 4C, respectively. This considerable reduction in d_p (by more than 25%) occurs within a radial distance of ~0.5 mm at that height. Unfortunately, aggregate statistics could not be obtained because of the apparent aggregate overlap in Fig. 4B.

Figure 5 displays two TEM micrographs of soot aggregates collected from the soot annuli of two separate flames (A in 1-g, B in 0-g). The burner exit conditions for these two flames were identical and corresponded to Case IV in Table 1. Each soot sample was collected at the height where the overall maximum value of f_v was measured in that particular flame. This height was Z = 10 mm in 1-g [5], and Z = 15 mm in 0-g. In essence, the soot aggregates seen in Fig. 5 represent the maximum primary sizes in these two flames. While no conclusive statement can be made regarding the degree of aggregation of the two samples (the aggregates in Fig. 5B probably overlap), it is apparent that the soot primary size in 0-g is considerably larger than that under buoyant conditions. The values of d_p were measured at the flame locations corresponding to the aggregates of Figs. 5A (1-g) and 5B (0-g). They were, respectively, 28.6 nm (σ_g = 3.9 nm) and 40.6 nm (σ_g = 5.4 nm). The increase of soot primary size in the absence of

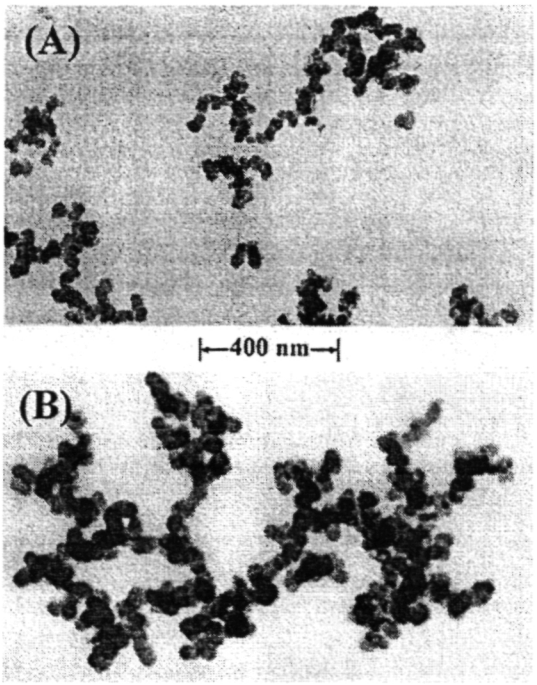

Fig. 5. Transmission electron micrographs of soot aggregates collected from the soot annuli of two separate flames (A in 1-g, B in 0-g). The burner exit conditions for these two flames were identical and corresponded to Case IV of Table 1. Each sample was collected at the height where the overall maximum value of f_v was measured in that particular flame. This height was $Z = 10$ mm for (A), and $Z = 15$ mm for (B).

gravity is consistent with the observations of Ku et al. [18] who sampled propane and ethylene flames. Finally, it is worth noting that the maximum value of d_p in 0-g for the diluted acetylene fuel used in the current work is almost identical to the soot primary size reported in [7] for aggregates released by an ethylene flame burning in 0-g.

The simultaneous knowledge of the local values of soot primary size and soot volume fraction for the flame aerosol can produce [26] estimates of the local values of the number concentration of primary particles (N_p) and surface area (S_T) of particulate phase per unit volume of the combustion gases according to the expressions

$$N_p = \frac{6f_v}{\pi d_p^3}, \quad S_T = \frac{6f_v}{d_p}$$

These simple expressions are based on two main assumptions. The first requires point contact between the monodisperse spherical primary particles forming the polydisperse aggregates. Since the soot aggregates consist of primary particles bridged together (see Fig. 5), the calculated value of S_T forms an *upper bound* of the actual soot surface area. The second assumption requires that particle nucleation is not active during the soot surface growth period. The observed local uniformity of d_p supports the latter condition. Table 2 lists the values of N_p and S_T determined for the two radial locations corresponding to Figs. 4B and 4C; both at $Z = 15$ mm, where the overall peak value of soot volume fraction was measured for Flame IV in 0-g. The primary particle number density N_p is about the same at both radial locations, thus suggesting nucleation rates of similar strength at the beginning of the corresponding flow paths lower in the flame. On the other hand, the soot surface area is reduced away from the soot annulus at that height. One set of 1-g values for N_p and S_T is given in Table 2 for the soot annulus of

TABLE 2

Selected Data for the Soot Aerosol

Flame	Height (mm)	Radial Location (mm)	f_v (ppm)	d_p (nm)	N_p (cm^{-3})	S_T (cm^2/cm^3)
IV in 0-g	15	2.3[a]	11.1	40.6	3.2×10^{11}	16.4
IV in 0-g	15	2.8[b]	5.7[d]	29.9	4.1×10^{11}	11.4
IV in 1-g	10	1.6[c]	7.9[d]	28.6	6.4×10^{11}	16.6

[a] Soot annulus.
[b] Outside soot annulus.
[c] Soot annulus.
[d] From [5].

Flame IV at the height Z = 10 mm, where the overall maximum value of soot volume fraction was measured [5]. The number density of the primary particles in 1-g is by a factor of 2 higher than that in 0-g, suggesting relatively stronger nucleation rates in the presence of buoyancy. On the other hand, under the conditions investigated in the current study, buoyancy appears to exert little influence on soot surface areas. Finally, it is worth mentioning that the measured values of N_p and S_T for the 50% (vol.) C_2H_2-N_2 fuel mixture in this study are similar to those reported in [26] for buoyant ethylene flames.

CONCLUSIONS

The spatial distributions and morphological properties of the soot aerosol have been examined experimentally in a series of soot-emitting 0-g laminar gas-jet nonpremixed flames, which have characteristic flow residence times varying by up to a factor of 2. The work was performed at the 2.2-s drop tower of the NASA Lewis Research Center. The experimental methodology deployed jet diffusion flames of nitrogen-diluted acetylene fuel burning in quiescent air at atmospheric pressure. Full-field laser-light extinction was utilized to determine transient soot spatial distributions in the cylindrical flames, and thermophoretic sampling was employed in conjunction with TEM to define soot microstructure and primary sizes at selected locations within the flames. The 50% (volume) C_2H_2/N_2 fuel mixture was injected through mm-sized burners with Reynolds numbers of the order of 100. While the 0-g flames released soot from their open tip, their buoyant counterparts operated below their smoke point.

The 0-g flames attained a quasi-steady state roughly 0.7 s after ignition, and sustained their annular structure even beyond their luminous flame tip. The gas-jet momentum at the burner exit proved to be an influential parameter affecting the spatial distribution of the soot field in 0-g (contrary to buoyant-flame structure). The measured peak soot volume fractions showed a complex dependence on burner exit conditions, and decreased in a nonlinear fashion with decreasing flow residence times. Fuel preheat by ~140 K appears to accelerate the formation of soot near the flame axis via enhanced fuel pyrolysis rates. In turn, the increased soot presence triggers higher flame radiative losses (i.e., reduced flame temperatures) which may account for the observed premature suppression of soot growth along the annular region.

Electron photomicrographs of soot samples collected thermophoretically from a 0-g flame which featured a burner exit velocity typical of buoyant combustion conditions, revealed the presence of soot precursor particles near the symmetry axis at an axial location around mid-flame height. At that height, the experimental observations also verified that soot primary sizes are nearly uniform locally, but vary considerably with radius. A reduction of primary size by more than 25% was measured along a radial increment of ~0.5 mm from the radial location of the soot annulus. The peak value of soot primary size in 0-g was found to be by 40% larger than in 1-g, under the same burner exit conditions.

Estimates of the number concentration of primary particles and surface area of soot particulate phase per unit volume of the combustion gases were also made for selected in-flame locations. The number density of primary particles in 1-g was by a factor of 2 higher than that in 0-g, suggesting relatively stronger nucleation rates in the presence of buoyancy. On the other hand, under the conditions investigated in the current study, buoyancy appeared to exert little influence on soot surface areas.

This work has been supported by NASA under Grant No. NGT3-52300. The authors wish to thank Prof. Mun Choi and Kirk Jensen of UIC for the conveyance of the tomographic inversion programs.

REFERENCES

1. Law, C. K., and Faeth, G. M., *Prog. Energy Comb. Sci.* 20:65–113 (1994).
2. Bahadori, M. Y., Edelman, R. B., Stocker, D. P., and Olson, S. L., *AIAA J.* 28:236–244 (1990).
3. Mortazavi, S., Sunderland, P. B., Jurng, J., Köylü, Ü. Ö., and Faeth, G. M., 31st Aerospace Sciences Meeting, Reno NV, Jan. 1993, Paper AIAA 93-078.
4. Megaridis, C. M., Konsur, B., and Griffin, D. W., *Twenty-Sixth Symposium (International) on Combus-*

tion, The Combustion Institute, Pittsburgh, 1996, pp.1291–1299.
5. Konsur, B., Megaridis, C. M., and Griffin, D. W., *Combust. Flame* 116:334–347 (1999).
6. Greenberg, P. S., and Ku, J. C., *Combust. Flame* 108:227–230 (1997).
7. Urban, D. L., Yuan, Z.-G., Sunderland, P. B., Linteris, G. T., Voss, J. E., Lin, K. C., Dai, Z., Sun, K., and Faeth, G. M., 36th Aerospace Sciences Meeting, Reno NV, Jan. 1998, Paper AIAA 98-0568.
8. Lekan, J., Gotti, D. J., Jenkins, A. J., Owens, J. C., and Johnston, M. R. (1996). *Users Guide for the 2.2 Second Drop Tower of the NASA Lewis Research Center.* NASA TM-107090.
9. Greenberg, P. S., and Ku, J. C., *Appl. Optics* 36:5514–5522 (1997).
10. Dasch, C. J., *Appl. Optics* 31:1146–1152 (1992).
11. Smyth, K. C., and Shaddix, C. R., *Combust. Flame* 107:314–320 (1996).
12. Köylü, Ü. Ö., Faeth, G. M., Farias, T. L., and Carvalho, M. G., *Combust. Flame* 100:621–633 (1995).
13. Dobbins, R. A., and Megaridis, C. M., *Langmuir* 3:254–259 (1987).
14. Rosner, D. E., Mackowski, D. W., and Garcia-Ybarra, P., *Combust. Sci. Technol.* 80:87–101 (1991).
15. Honnery, D. R., and Kent, J. H., *Combust. Flame* 82:426–434 (1990).
16. Mauss, F., Schäfer, T., and Bockhorn, H., *Combust. Flame* 99:697–705 (1994).
17. Megaridis, C. M., and Dobbins, R. A., *Combust. Sci. Technol.* 71:95–109 (1990).
18. Ku, J. C., Griffin, D. W., Greenberg, P. S., and Roma, J., *Combust. Flame* 102:216–218 (1995).
19. Köylü, Ü. Ö., *Combust. Flame* 109:488–500 (1997).
20. Santoro, R. J., Yeh, T. T., Horvath, J. J., and Semerjian, H. G., *Combust. Flame* 53:89–115 (1987).
21. Dobbins, R. A., and Subramaniasivam, H., in *Soot Formation in Combustion* (H. Bockhorn, Ed.), Springer-Verlag, Berlin, 1994, pp. 290–301.
22. Dobbins, R. A., Govatzidakis, G. J., Lu, W., Schwartzman, A. F., and Fletcher, R. A., *Combust. Sci. Technol.* 121:103–121 (1996).
23. Julien, R., and Botet, R., *Aggregation and Fractal Aggregates*. World Scientific, Singapore, 1987.
24. Dobbins, R. A., and Megaridis, C. M., *Appl. Optics* 30:4747–4754 (1991).
25. Köylü, Ü. Ö., and Faeth, G. M., *J. Heat Transfer* 116:152–159 (1994).
26. Megaridis, C. M., and Dobbins, R. A., *Combust. Sci. Technol.* 66:1–16 (1989).

Received 2 July 1998; revised 5 February 1999; accepted 11 February 1999